J. Am. Chem. Soc. **1981**, *103*, 7074–7084

Neophyl Rearrangements in Crystalline Bis(3,3,3-triphenylpropanoyl) Peroxide. 2. Structural Studies by X-ray and EPR. The Mechanistic Role of Inert Molecules[1]

Donald W. Walter and J. Michael McBride*

Contribution from the Department of Chemistry, Yale University, New Haven, Connecticut 06511. *Received November 12, 1980*

Abstract: The threefold degeneracy in rearrangement of 2,2,2-triphenylethyl radical (T) to 1,1,2-triphenylethyl radical (R) is lifted for radical pairs generated by photolysis of the crystalline benzene solvate of the title compound (TPPP). X-ray structure determination of the solid is reported, and bond-angle distortions in the triphenylethyl group are analyzed. The conformation of TPPP should favor rearrangement of one of the three phenyls, but intermolecular influences (particularly from the CO_2 generated during photolysis) should favor rearrangement of a different phenyl. Zerofield splitting and hyperfine splitting tensors of the six radical pair intermediates in this system are interpreted to supply considerable structural detail on the course of the rearrangements. Very little atomic motion occurs (even during neophyl rearrangement) until the ultimate disappearance of radicals. It is shown that in the initial, strained geometry of the pair of T radicals the intermolecular influence of CO_2 is dominant in controlling rearrangement, but that when the strain is relaxed, molecular conformation becomes dominant. A scheme is proposed for classifying environmental influences on solid-state reactions, and it is shown that the strong effects on these radical pairs, although without much precedent, could be important in many other reactions.

Structural studies of single crystals by X-ray diffraction are uniquely valuable both for what they reveal about the nature of the solid state and for the insights they provide into molecular structure. These insights have been useful for understanding molecules in fluid phases. One would expect that structural studies of a series of reaction intermediates in a single crystal should be similarly valuable both for discovering the special factors which govern solid-state reactions and for gaining insights into molecular reactivity. The latter should help us understand solution and gas-phase chemistry.[2] In the present work single-crystal EPR spectroscopy was used in the structural study of a free-radical rearrangement.

A special feature of solid-state chemistry is the possibility of lifting the degeneracy among a number of seemingly equivalent reaction pathways. In solution the neophyl rearrangement of the 2,2,2-triphenylethyl radical (T) to 1,1,2-triphenylethyl (R) is

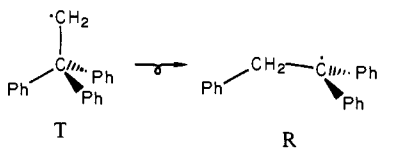

T R

probably degenerate in the sense that three chemically equivalent phenyl groups are available for migration to the primary center. The chemical equivalence may derive either from static threefold symmetry (assuming rapid rotation of the methylene group) or from rapid equilibration among a symmetric set of three unsymmetric conformations, each with three different torsional angles about the bonds joining the phenyl rings to the central carbon. The latter source may be the more likely, since X-ray diffraction has shown that among triphenylmethane and related trityl compounds, only the bromide and the chloride approximate threefold symmetry in the solid state.[3] There is no more reason to expect instantaneous site symmetry in solutions than in crystals, although time averaging may be faster. The general absence of symmetry in precursors of T suggests that, if conformational equilibration among the phenyl groups in the solid state is slower than neophyl rearrangement, the degeneracy should be lifted, and migration of one of the three phenyl groups should predominate.

In the preceding paper we reported using kinetic information from single-crystal EPR spectra of photolyzed bis(3,3,3-triphenylpropanoyl) peroxide (TPPP) to demonstrate that the crystalline matrix retards rearrangement of T to R by a substantial factor.[4] We hoped to use the structural information in these spectra, together with X-ray studies of the peroxide host lattice, to identify rearrangement products in situ, where products from migration of the different phenyl groups could still be distinguished. The structural picture which emerged not only demonstrates the anticipated selectivity among degenerate rearrangement pathways, but also suggests that CO_2, a seemingly inert byproduct of radical generation, plays a crucial mechanistic role in the subsequent rearrangement.

In discussing the role of CO_2, it will be useful to distinguish between "chemical" and "physical" modes of lattice steric influence on solid-state reaction. In the chemical mode intermolecular forces are important in determining the activation energy of the reaction step which involves a change of bonding. In the physical mode the only important forces in the transition state

(1) Based on the Ph.D. Thesis of D. W. Walter, Yale University, 1980. Presented in part at the 15th Conference on Reaction Mechanisms, Colorado State University, Ft. Collins, CO, June 28, 1974, and at the Fifth International Symposium on Chemistry of the Organic Solid State, Brandeis University, Waltham, MA, June 13–16, 1978.

(2) See, for example: Dunitz, J. D. "X-Ray Analysis and the Structure of Organic Molecules"; Cornell University Press: Ithaca, N.Y., 1979.

(3) The Cambridge Crystallographic Data Base contains 13 examples of Ph_3CX. We list X together with the range of the three torsional angles (deg) between phenyl and C–X, as a measure of the departure from threefold symmetry. Entries are keyed by letter to the following reference list. Multiple angle entries for a substituent refer to crystallographically independent molecules. For X = Cl, the groups are *p*-anisyl instead of phenyl; for X = NF_2, one of the phenyl groups has a *p*-bromo substituent. (a) Br, 0, 0, 0; (b) Cl, 3; (c) H, 23, 24; (d) OH, 24; (e) $OOCPh_3$, 35; (f) F, 42; (g) NF_2, 51; (h) NPh_2, 59; (i) $CHPh_2$, 59, 74; (j) Ph, 61. (a) Stora, C.; Poyer, N. *Bull. Soc. Chim. Fr.* **1966**, 841. (b) Dunand, A.; Gerdil, R. *Acta Crystallogr., Sect. B* **1976**, *B32*, 1591. (c) Rieche, C.; Pascard-Billy, C. *Ibid.* **1974**, *B39*, 1874. (d) Stora, C. *Bull. Soc. Chim. Fr.* **1971**, 2153. (e) Glidewell, C.; Liles, D. C.; Walton, D. J.; Sheldrick, G. M. *Acta Crystallogr., Sect. B* **1979**, *B35*, 500. (f) Takusagawa, F., et al. *Cryst. Struct. Commun.* **1976**, *5*, 753. (g) Surles, J. R.; Bumgardner, C. L.; Bordner, J. *J. Fluorine Chem.* **1975**, *5*, 1975. (h) Hoekstra, A.; Vos, A. *Acta Crystallogr., Sect. B* **1975**, *B32*, 1716. (i) Destro, R.; Pilati, T.; Simonetta, M. *J. Am. Chem. Soc.* **1978**, *100*, 6507. (j) Robbins, A., et al. *Acta Crystallogr., Sect. B* **1975**, *B31*, 2395.

(4) Walter, D. W.; McBride, J. M. *J. Am. Chem. Soc.*, preceding paper in this issue.

0002-7863/81/1503-7074$01.25/0

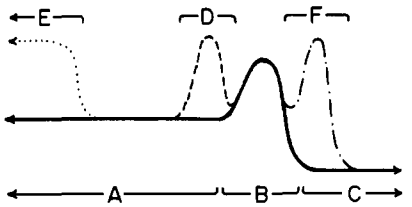

Figure 1. Representation of the potential energy surface for a gas-phase reaction, indicating regions where increases in relative energy on passing to the solid state would have different effects on the reaction rate. A, B, and C are starting material, transition state, and product, respectively. Continuation of A and C to the left and right indicates the possibility for a large region on the surface which may border transition states for other reactions. Region D is a part of A near B; region E is a part of A remote from B, but perhaps near a transition state for a competing reaction of A; region F is part of C near B.

for change of bonding are intramolecular, as they might be in the gas phase or in a low-pressure liquid, and the lattice can be influential only through inhibiting changes in molecular position or conformation which precede or follow the changes in bonding.

Neuman's study of the decomposition rates for one- and two-bond initiators at high pressure illustrates a distinction between chemical and physical influences in solution chemistry.[5] For two-bond initiators the pressure influence is purely chemical and results from inhibiting the increase in molecular volume during bond cleavage. For one-bond initiators there is in addition a physical influence, which results from the volume of activation for diffusive separation of the reversibly formed radical pair. This effect is physical because no change of bonding occurs in the step affected. Diffusion-limited reaction rates are the most common example of physical influence.

A brief general discussion of how steric interaction with a rigid matrix changes the shape of a gas-phase potential-energy surface may help clarify the distinction we see between chemical and physical influences.

The most important changes in the *shape* of the surface should be due to repulsive potentials. Attractive potentials lower the surface as a whole on going from vapor to condensed phase (by the sublimation energy), but intermolecular attraction varies relatively slowly with atomic position and spans a limited range of energies, so its stabilization of different regions of the surface should be similar. When transition states are more polarizable than ground states, they should be preferentially stabilized by van der Waals attraction, but even this effect is small compared with the magnitude of repulsion between nonbonded atoms at short distances. In the present discussion we consider only repulsive potentials. It would be simple to expand the discussion to include consideration of attractive potentials.

Figure 1 represents the potential energy surface for a gas-phase reaction, where A, B, and C, respectively, denote starting material, a particular transition state, and the corresponding product. D and E are subregions of starting material, which are, respectively, near to and far from transition state B. F is a subregion of product near B. We now consider how reactivity should be affected when each of these regions in turn is raised in energy by the nonbonded repulsion which results from misfit into a rigid lattice. In practice several of the regions would probably be affected simultaneously.

Raising the energy of region A should accelerate the reaction by decreasing the enthalpy of activation. Since molecules usually pack into a crystal in a geometry which gives an energy minimum, at least locally, it might seem that it would be rare for the starting material to be selectively destabilized. However, for molecules near crystal defects, or for intermediates generated in a "hostile" environment by preliminary exothermic reaction of the host substance, or for photoexcited molecules, acceleration due to this "type A" effect might be anticipated. A type A effect may be important in the present study.

Raising the energy in region B, the region of the chemical reaction barrier, should reduce the rate by increasing the enthalpy of activation, or, if only enough of the surface is raised to narrow the pass between A and C, by decreasing the entropy of activation. It seems likely that many solid-state reactions are slow for this reason, since the transition state should not in general fit easily into a cavity which was designed to minimize the energy of the starting material. However, the type B effect is difficult to distinguish experimentally from the type D or type F effects described below.

Raising the energy in region C should not affect the rate of the forward reaction until the product becomes less stable than the former transition state. A type C effect could influence the equilibrium constant of a reaction which is nearly thermoneutral (e.g., a change in conformation or hydrogen bonding), but for a typically exothermic reaction the product would simply accumulate in the hostile matrix until it was able to segregate into its own phase.[6]

Raising the energy in region D, as shown by the dashed line, to a level higher than that of region B should retard reaction by introducing a new transition state with higher enthalpy (or lower entropy) of activation. The distinction between a type D and a type B effect is that in the former there is no change in chemical bonding at the transition state for the matrix reaction. Type D is thus a physical effect. Type D effects are familiar in diffusion-controlled reactions and should be important whenever motion in the matrix is difficult relative to bond-making or -breaking. Insensitivity of solid-state reaction rate to an isotopic substitution which changes the solution rate is diagnostic of a type D effect.[7] In principle other sorts of substitution could also be used in this sort of test, but usually it will be almost impossible to correct for the accompanying changes in crystal packing.

Raising the energy of region E, as shown by the dotted line, can favor formation of C in two distinct ways. First, by decreasing the range of geometries accessible to starting material, the type E effect accelerates reaction through an increased entropy of activation. Second, by imposing new barriers between starting material and other products, the effect favors reaction to C competitively even without increasing its rate. It seems to us that most topochemical phenomena which have been observed can be explained as type E effects, and that most of these may be of the second kind. There are relatively few cases in which reaction is faster in the solid than it would be expected to be in the pure liquid at the same temperature.[8] Thus it is rarely necessary to invoke the first kind of type E effect.

In a sense this classification depends on point of view, because the second kind of type E effect is a type D (or possibly type B) effect for the competing reaction which is retarded.

Raising region F above B can also retard formation of product. This physical effect is like the type D effect and is very difficult to distinguish from it in the solid state, although Neuman's one-bond initiators constitute a solution analogue.[9]

Of all these types of lattice steric effects, only types A and B, and perhaps the first kind of type E, may be considered chemical. There are few known examples than fit into any of these three classes. Almost all effects which have hitherto been observed can be classed as type D or the second kind of type E. These are physical effects, since they do not directly affect the changes of bonding. We believe the influence of CO_2 in rearrangement of T is remarkable in that it represents chemical effects of types A and B.

Crystal Structure. TPPP crystallizes from benzene as thick plates of a triclinic solvate with two benzenes per peroxide and the following crystal data: $C_{42}H_{34}O_4 \cdot 2C_6H_6$, FW = 759.0; space group $P\bar{1}$; a = 9.821 (4), b = 9.924 (2), c = 12.610 (2) Å, α = 70.43 (1), β = 66.12 (3), γ = 80.02 (3)°; V = 1057.9 Å^3; ρ_{calcd}

(5) Neuman, R. C., Jr. *Acc. Chem. Res.* **1972**, *5*, 381.

(6) Paul, I. C.; Curtin, D. Y. *Acc. Chem. Res.* **1973**, *6*, 217.

(7) (a) McBride, J. M. *J. Am. Chem. Soc.* **1971**, *93*, 6302. (b) Skinner, K. J.; Blaskiewicz, R. J.; McBride, J. M. *Isr. J. Chem.* **1972**, *10*, 457.

(8) For example: Sukenik, C. N.; Bergman, R. G.; et al. *J. Am. Chem. Soc.* **1977**, *99*, 851.

(9) A likely solid-state example is photolysis of dibenzoyl peroxide at 5 K, which gives phenyl–benzoyloxyl, but not benzoyloxyl–benzoyloxyl, radical pairs. McBride, J. M.; Vary, M. W. *Tetrahedron*, in press.

Table I. Atomic Fractional Coordinates and Their Estimated Standard Deviations[a]

atom	x	y	z	atom	x	y	z
O1	0281 (2)	2235 (2)	−1057 (2)	C44	3068 (4)	4026 (4)	1802 (3)
O2	0804 (2)	0073 (3)	−0175 (3)	C45	1564 (4)	4302 (4)	2208 (3)
C1	1154 (3)	1362 (3)	−0790 (2)	C46	0649 (4)	3251 (4)	2592 (3)
C2	2769 (3)	1473 (3)	−1053 (2)	H1	279 (3)	164 (2)	−033 (2)
C3	3602 (3)	2646 (3)	−2238 (2)	H2	326 (3)	055 (2)	−110 (2)
C11	5286 (3)	2377 (3)	−2475 (2)	H12	502 (2)	220 (2)	−071 (2)
C12	5774 (3)	2201 (3)	−1541 (2)	H13	753 (3)	196 (3)	−103 (2)
C13	7271 (3)	2051 (3)	−1726 (3)	H14	934 (3)	203 (3)	−297 (2)
C14	8321 (3)	2085 (3)	−2846 (3)	H15	852 (3)	226 (3)	−453 (2)
C15	7872 (3)	2268 (4)	−3787 (3)	H16	608 (2)	252 (2)	−423 (2)
C16	6366 (3)	2405 (3)	−3605 (2)	H22	476 (2)	510 (2)	−378 (2)
C21	3225 (3)	4164 (3)	−2101 (2)	H23	434 (3)	743 (3)	−367 (2)
C22	3996 (3)	5305 (3)	−3052 (2)	H24	249 (3)	792 (3)	−184 (2)
C23	3743 (3)	6686 (3)	−2967 (3)	H25	129 (3)	605 (3)	−021 (2)
C24	2724 (3)	6969 (3)	−1921 (3)	H26	169 (3)	370 (2)	−039 (2)
C25	1983 (3)	5857 (3)	−0962 (2)	H32	228 (3)	446 (2)	−380 (2)
C26	2227 (3)	4469 (3)	−1049 (2)	H33	165 (3)	404 (3)	−520 (2)
C31	3220 (3)	2471 (3)	−3259 (2)	H34	208 (3)	178 (3)	−553 (2)
C32	2500 (3)	3541 (3)	−3907 (2)	H35	333 (3)	−006 (3)	−452 (2)
C33	2108 (3)	3306 (4)	−4773 (3)	H36	402 (2)	041 (2)	−308 (2)
C34	2386 (3)	2001 (4)	−4981 (2)	H41	060 (3)	113 (3)	257 (3)
C35	3096 (3)	0914 (3)	−4340 (2)	H42	313 (3)	073 (3)	197 (2)
C36	3514 (3)	1161 (3)	−3504 (2)	H43	479 (3)	240 (3)	140 (3)
C41	1215 (4)	1916 (4)	2389 (3)	H44	363 (3)	466 (3)	160 (3)
C42	2731 (4)	1648 (4)	1980 (3)	H45	114 (4)	531 (4)	233 (3)
C43	3669 (4)	2710 (4)	1681 (3)	H46	−044 (4)	350 (4)	277 (3)

[a] ×10³ for hydrogen, ×10⁴ for other atoms. Atoms of the aromatic rings are indexed according to ring number and position in the ring.

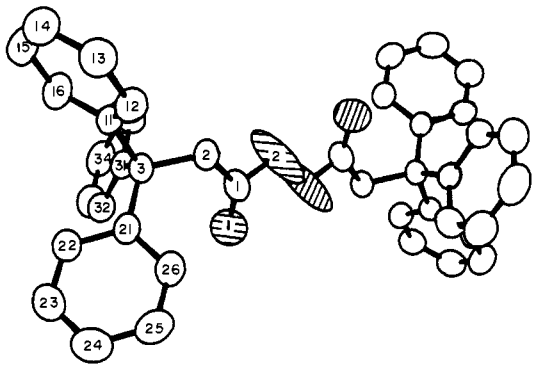

Figure 2. ORTEP plot of TPPP in the benzene solvate. Oxygen atoms are denoted by shading. In two-digit atom numbers the first digit denotes ring number and the second denotes position in the ring. Carbons 33, 35, and 36 are partially hidden by carbons 32, 11, and 12, respectively. Thermal ellipsoids are outlined to include 50% probability.

Table II. Selected Bond Lengths (Å) and Angles (deg)[a]

	Lengths[b]		
O1-C1	1.175	C2-C3	1.560
O2-O2′	1.476	C3-C11	1.548
C1-C2	1.499	C3-C21	1.538
O2-C1	1.276	C3-C31	1.546
	Angles		
O2′-O2-C1	110.0	C3-C11-C12	119.4
O1-C1-O2	121.8	C3-C11-C16	123.2
O1-C1-C2	130.4	C12-C11-C16	117.2
O2-C1-C2	107.9	C3-C21-C22	118.9
C1-C2-C3	115.4	C3-C21-C26	124.0
C2-C3-C11	106.9	C22-C21-C26	117.0
C2-C3-C21	112.7	C3-C31-C32	123.0
C2-C3-C31	106.9	C3-C31-C36	119.7
C11-C3-C21	105.2	C32-C31-C36	117.2
C11-C3-C31	112.2		
C21-C3-C31	112.9		

[a] The estimated standard deviations in lengths are 0.003 Å, and in angles 0.2 deg. [b] Aromatic C-C distances ranged from 1.356–1.395 Å.

= 1.191 g/cm³ for $Z = 1$. The largest face is usually (001), but the following faces are also commonly observed: (100), (010), (110), (101), (011), ($\bar{1}$10), (102), and (112). The solvate is stable for many months in the refrigerator in an atmosphere saturated with benzene but after a day on the bench top, a microscope reveals solvent loss as woolly structures growing into the transparent crystal from some areas of the surface.

Table I presents atomic coordinates based on 2243 unique room-temperature X-ray structure factors ($\sin\theta/\lambda < 0.517$) and an unconstrained model with thermal parameters that are isotropic for hydrogen and anisotropic for carbon and oxygen. The final value of $R = \sum||F_o| - |F_c||/\sum|F_o|$ was 0.05. The molecular structure and numbering scheme are shown in Figure 2. Selected bond distances and angles are presented in Table II. More complete tabulations of distances, angles, planes, torsional angles, and intermolecular distances from the peroxide group, as well as of structure factors and thermal parameters, are available as Supplementary Material. All principal values of root mean square thermal vibrational amplitudes are between 0.17 and 0.40 Å, except for those of the peroxide oxygen, O2, which has principal values of 0.15, 0.22, and 0.74 Å. The out-of-plane direction of the largest axis suggests disorder (see Figure 2), but the neighboring atoms show normal temperature factors, and the O–O distance (1.476 Å) is close to 1.470 Å, the average for 24 O–O bonds of organic peroxides in the Cambridge Crystallographic Data Base.[10] The largest seven peaks in the final difference Fourier synthesis (0.2 to 0.4 e/Å³) are all within 1.6 Å of the carboxyl group.

EPR Tensors. Single-crystal EPR spectra commonly provide structural information through the anisotropy of g shifts and of proton hyperfine splitting (hfs). For these hydrocarbon radicals g-shift anisotropy was too small to measure and interpret, but the hfs tensors were informative. Since all of the signals came from pairs of free radicals, additional information was available from the zerofield splitting (zfs), which results from magnetic dipolar coupling between the electron spins of the two radicals.

zfs. For each of the radical pairs in Scheme I of ref 4 the doublet splitting was determined for 40 to 168 magnetic field directions, chosen where possible to cover all directions within a hemisphere in a crystal-fixed coordinate system. The field direction was varied by rotating the crystal in 10 to 20° steps about each of 7 or 8 axes, corresponding to different mountings on the

(10) These 24 C–O–O–C fragments were chosen from structures refined to $R < 0.12$. The O–O distances range from 1.445–1.490 Å and have an rms deviation of 0.014 Å from their 1.470 Å mean.

Table III. Radical-Pair zfs Tensors

radical pair[a]	no. of mountings[b]	no. of observations[c]	rms dev,[d] G	eigenvalue,[e] G	eigenvector ($\times 10^4$)[f] a	b'	c^*	angular err, deg
				−223.4 (9)	8078	4027	−4305	<1
TT*	9	168	4.1	110.1 (10)	4893	−8653	1086	8
				113.3 (6)	3288	2983	8960	8
				−236.7 (12)	8142	3929	−4274	<1
TT	8	130	4.3	116.7 (10)	−5709	6756	−4664	15
				120.0 (9)	1055	6238	7744	15
				−88.3 (4)	7529	4202	−5066	1
TR_3 (d_{34})	8	114	1.3	43.0 (3)	−1662	8661	4714	5
				45.3 (2)	6368	−2707	7219	5
				−44.6 (4)	7084	4653	−5308	1
R_3R_3 (d_{34})	4	53	1.1	21.5 (5)	−2599	8710	4168	9
				23.2 (4)	6563	−1573	7379	9
				−137.4 (5)	6138	4514	−6477	<1
TR_1 (d_4)	8	83	1.9	63.9 (5)	5335	3675	7618	3
				73.4 (6)	−5819	8131	0153	3
				−64.7 (9)	5672	4600	−6832	1
R_3R_1 (d_4)	4	40	2.1	28.6 (9)	7196	1267	6827	5
				36.2 (7)	−4006	8789	2592	5

[a] Where deuterated samples were used, the extent of labeling is given in parentheses. [b] Each rotated through 180° in steps of 10° to 20°. [c] Total number of different splittings measured. [d] Root mean square difference between observed splittings and those calculated from the refined tensor. [e] These eigenvalues of spectral splittings are 3 times the corresponding D tensor elements. [f] Direction cosines ($\times 10^4$) referred to an orthonormal system with a along crystallographic a, b' in the ab plane near b, and c^* along the reciprocal c axis. This system was used for all EPR work.

goniometer rod. Traceless zfs tensors were fit to these data assuming high-field electron spin quantization, since zfs was too small to require second-order corrections. Table III presents the diagonalized zfs tensor for each of the six radical pairs together with an indication of the precision of the fit and of the number of field directions and of crystal mountings that were used. Errors in the tensors were estimated by least-squares refinement with field directions expressed in a coordinate system in which preliminary refinement has shown the tensor to be diagonal. The covariance matrix gave estimated standard deviations for each tensor element. Those of the diagonal elements are reported as eigenvalue errors. Angular errors of eigenvector orientation were estimated by the change in eigenvector direction when off-diagonal zero elements were replaced by their estimated standard deviations and the tensor was diagonalized again.

In every case the tensor was so near to cylindrical symmetry that the choice of eigenvalue signs was obvious from a simple model with two localized electron spins, but the departure from axial symmetry was always statistically significant. The experimental reliability of as small an eigenvalue difference as between 43.0 and 45.3 G (TR_3) can be judged by Figure 3, which plots the maximum positive splitting observed in each crystal mounting against the angle of the corresponding magnetic field in the crystal-fixed plane perpendicular to the direction of maximum negative zfs. Proximity of the experimental points to the sine-squared curve from the fitted tensor confirms the error estimates for the positive eigenvectors. This type of plot provides a valuable check, because it is insensitive to the systematic influence of small errors in crystal mounting angles.

hfs. There are two important differences in hfs between the EPR spectra of radical pairs and those of the isolated radicals. The hfs in radical pairs is only half as large as in the corresponding isolated radicals, and one of the $\Delta m = 1$ transitions of the radical pair is less sensitive to second-order complication of the hfs than are the transitions of the isolated radicals. The other is more sensitive.

The first effect results because in the high-field limit the T_0 member of the triplet state, with no magnetization in the field direction, is not subject to hfs. The T_{-1} and T_1 components of a radical pair have the same local electron spin densities as would the isolated radicals. Since both initial and final states of the EPR transitions of isolated radicals are subject to hfs, the observed hfs

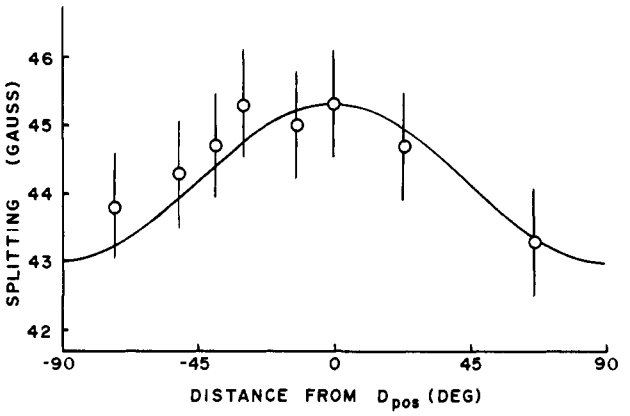

Figure 3. Maximum positive zfs of TR_3 for each of 8 rotations about different axes of a TPPP-d_{30} crystal plotted against the field direction at which the maximum occurred. The direction is given by the angle from the largest positive eigenvector of the zfs tensor of Table VI. The curve is calculated from that tensor, and error bars indicate the estimated uncertainty in measuring the splitting of these relatively broad lines.

in the $T_{-1} \rightarrow T_0$ and $T_0 \rightarrow T_1$ transitions of the pair is only half as large.

Second-order effects become important when the Zeeman field ($-g_N\beta_N H$) and the isotropic hyperfine field at a nucleus a·**S**, where **S** is the electron spin) cancel one another, so that anisotropic hyperfine components perpendicular to the applied field can make significant contributions to the net field at the nucleus. For the T_{-1} level when $a_{iso} > 0$ (or for T_1 when $a_{iso} < 0$) the Zeeman and isotropic hfs fields reinforce one another and suppress the second-order effects of modest hfs anisotropy.

For each hfs that we could measure in the radical pairs from TPPP we fit a tensor to the observed splittings in the two $\Delta m = 1$ transitions separately without second-order correction. Although hfs differences between the two transitions were small, both in the quality of the fit and in the derived tensors, Table IV records only the tensor which was less sensitive to second-order effects. The α-proton hfs tensors from TT* and TT were readily determined, because the lines were strong and sharp, and the large zfs of these pairs minimized problems from overlap.[4] Problems from weak, broad, and overlapping lines, even in appropriately deu-

Table IV. Radical-Pair hfs Tensors

radical pair[a]	protons[b]	data[c]	a_{iso}[d]	anisotropic eigenvalue[d,e]	eigenvector (×10⁴)[f] a	b′	c*	angular err, deg
		8		−3.6 (1)	−2752	−5126	8133	1
TT*	4α	113	−10.8	1.3 (1)	9566	−0618	2848	2
		0.3		2.3 (1)	−0958	8564	5074	2
		8		−3.7 (1)	−2161	−5397	8136	1
TT	4α	97	−10.6	1.3 (1)	9763	−1320	1718	3
		0.4		2.4 (1)	−0147	−8314	−5554	3
		4		−3.1 (2)	−4256	−3144	8485	3
TR_3 (d_{30})	2α	53	−11.2	1.5 (2)	0595	9260	3729	25
		0.4		1.7 (2)	9030	−2092	3754	25
		8		1.1 (1)	−6598	−5531	5087	9
TR_3 (d_{30})	$1\beta_1$	71	5.5	−0.5 (1)	4528	−8329	−3183	24
		0.2		−0.7 (1)	5997	0203	8000	23
		8		1.8 (1)	−7482	−5152	4181	6
TR_3 (d_{30})	$1\beta_2$	64	1.1	−0.7 (2)	6623	−5416	5177	26
		0.2		−1.1 (2)	−0402	6643	7464	26
		5		0.7 (2)	3195	−6668	−6733	37
TR_1 (d_{30})	$1\beta_1$	36	6.9	0.4 (2)	6345	−3772	6746	36
		0.3		−1.1 (1)	−7038	−6428	3025	12

[a] Where deuterated samples were used, the extent of labeling is given in parentheses. [b] Number of protons giving rise to the splitting and their position. [c] Number of crystal mountings, number of orientations measured, and rms deviation between observed splittings and those calculated from the fitted tensor (in gauss). [d] hfs in gauss for the triplet pair. Should be doubled for comparison with splittings in isolated radicals. [e] Estimated standard deviation in parentheses. [f] See Table III, footnote *f*.

terated samples, made the other hfs tensors difficult to determine, and in particular prevented us from determining the full α-proton tensor of TR_1.

Errors in the magnitude and direction of hfs were estimated as they were for zfs.

Discussion

Molecular Structure of TPPP. Although the bond distances, angles, and torsional angles of TPPP are not extraordinary, two aspects of its geometry merit discussion because they are particularly relevant to reaction in the crystal. These are the conformation of the acyl peroxide group and that of the triphenylethyl group.

The molecular center of symmetry imposes a C–O–O–C torsional angle of 180°, while most acyclic organic peroxides have angles of 104 ± 23°.[11] TPPP is not unique, however, since bis(triphenylmethyl) peroxide[3e] and bis(3,5-dimethylbenzoyl) peroxide[11] are also centrosymmetric in the solid state. The 176.4° torsional angle for C2–C1–O2–O2′ makes the eight atoms comprising the CO_2 groups and the methylene carbons effectively coplanar. This means that at 5.81 Å the incipient radical centers are as remote from one another as is conformationally possible, and that the incipient CO_2 molecules are positioned to provide maximum hindrance to radical recombination. In the twisted conformations of most other diacyl peroxides the CO_2 molecules are generated off the line of centers of the radical pair.

Figure 2 shows that the triphenylethyl group of TPPP departs from propeller symmetry. The role of the carbonyl group in determining this conformation is most easily appreciated by reference to a hypothetical conformation in which all three phenyls eclipse the C3–C2 bond. In a group as congested as triphenylethyl some eclipsing is unavoidable, but there are two reasons why several phenyls should not eclipse the same bond. First, there would be severe back strain among the ortho substituents remote from the eclipsed bond, and second, there would be a buttressing of the eclipsed interactions. In TPPP rings 1 and 3 twist away from the C3–C2 bond, but it would be difficult for ring 2 to twist in the same sense because of the proximity of C26 to O1 (3.17 Å). Furthermore, torsion of rings 1 and 3 removes the driving force for torsion of ring 2. The back strain on C22 is reduced, and since C3–C2 is no longer buttressed, the C2–C3–C21 angle opens by 3° to reduce the eclipsing strain. The bond angle within the ring at C21 narrows to 117°, and its exocyclic bond angles distort from their average by 2.5° (to 118.9 and 124.0°). This reduces the eclipsing strain still further, so that the C2–C26 eclipsed distance (2.930 Å) is only 0.008 Å shorter than C22–C11.

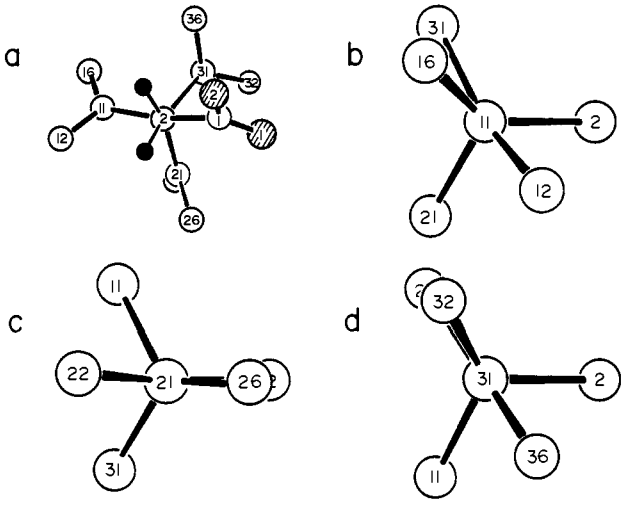

Figure 4. Conformation of the four bonds to C3, the central carbon of TPPP, as shown by projection from each of its substituent atoms. Carbon atoms are open circles of radius 0.3 Å. Oxygen atoms are shaded; hydrogen atoms, filled. (a) Projection from C2, the incipient radical carbon. (b–d) Projections from rings 1, 2, and 3, respectively, including the ortho carbons of the nearest ring.

The four parts of Figure 4 show the torsions about each of the four bonds to C3 by projections toward C3 from C2, C11, C21, and C31. Figure 4a shows that the twist of ring 3 allows 14° torsion from a staggered conformation about C2–C3 to increase the distance between ring 2 and the offending carbonyl group (C1–O1). Figures 4b, 4c, and 4d show the torsions of the phenyl groups. In each case phenyl very nearly eclipses one of the bonds from C3, and eclipsing strain is reduced by narrowing the ring

(11) This range holds for 8 of the 9 acyclic C–O–O–C fragments in the Cambridge Crystallographic Data Base. The exception is bis(triphenylmethyl) peroxide.[3e] In unpublished work in this laboratory, B. Segmueller, M. W. Vary, R. S. Miller, and R. A. Merrill have determined the torsional angles for eight other compounds of the type R–CO–O–O–CO–R′. When R = R′ these are: α-naphthyl, 91.2°; *o*-tolyl, 91.4°; *p-tert*-butylphenyl, 96.3°; *n*-decyl, 90.1°; 2-methyl-2-phenylpropyl, 82.0°; and 3,5-dimethylphenyl, 180°. Other cases include R = 2-chloro-2-phenylpropyl, R′ = 3-chlorophenyl, 82.9°; and di-*tert*-butyl diperoxyoxalate, 143.6°.

Table V. TPPP Torsional Angles Relevant to Rearrangement[a]

migrating ring	angle for attack by C2[b]	angle for radical stabilization by[c] ring 1	ring 2	ring 3
1	42.5 (0.54)		29.8 (0.75)	31.6 (0.73)
2	86.3 (0.00)	17.5 (0.95)		87.1 (0.00)
3	31.6 (0.73)	74.5 (0.07)	27.5 (0.79)	

[a] The number given in parentheses is the squared cosine of the angle. Overlap between the radical p orbital and the phenyl π system should go approximately as the cosine of the angle. If their interaction is proportional to overlap and small enough to be regarded as a perturbation, the energy shift should be proportional to the squared cosine. [b] Torsional angle in TPPP between the p orbital of the ipso carbon of the migrating ring and the C3-C2 bond. This should control overlap between the radical p orbital on C2 and the π system of the phenyl it attacks. [c] Torsional angle in TPPP between the p orbital of the ipso carbon of the indicated ring and the bond joining C3 to the migrating ring. This angle controls initial overlap between the breaking bond and the stabilizing phenyl.

angle at the ipso carbon to 117.1 ± 0.1°, by distorting its exocyclic angles by 2.1 ± 0.5°, and by increasing the relevant angle at C3 from tetrahedral to 112.5 ± 0.4° (in Figure 4b this angle is C11–C3–C31). The three angles at C3 which are not involved in eclipsing are 106.0 ± 0.9°. It has not previously been noted that tetraphenylmethane shows the same reasonable pattern of bond angle response to strain from torsional angles which, in its case, are within 9.6° of eclipsed.[3j] It has angles of 110.9° and 106.7° at the central carbon, a ring angle at the ipso carbon of 117.5°, and 5° distortion of the exocyclic angles.

There are two ways in which phenyl groups participate in the neophyl rearrangement of T, and thus two ways in which their torsional angles are important. One phenyl must migrate to the primary center, while the other two provide resonance stabilization for the rearranged radical. Although it is customary to draw structures suggesting that a phenyl moves *to* the primary center, this is misleading both in an isolated molecule, where angular momentum should be conserved, and in a rigid environment, where the shape of the radical should change as little as possible. In either case the dominant initial motion is the primary center's bending toward the ipso carbon of a phenyl ring to approach the geometry of a spirocyclopropane, which may or may not constitute a reaction intermediate. In order to form the third cyclopropane bond the attacked phenyl group must twist to eclipse the π orbital of its ipso carbon with the bond joining the central and radical carbons (C3–C2). It is crucial how small this torsional angle is in the radical and how readily it can approach zero.

Beyond the spiro geometry the other two phenyl groups stabilize the developing radical center to the extent that their π systems overlap the breaking bond, the one which links the migrating phenyl to the quaternary carbon (C3). From the spiro geometry it must be easier to proceed to the relatively stable product R than to return to T. This suggests that the rate-determining transition state comes before the spiro structure, whether or not it is an intermediate, and that susceptibility of the migrating phenyl to attack should be much more important than potential stabilization of the new radical center. Thus back strain, not product stabilization, explains why T rearranges more rapidly than the neophyl radical.

Figure 4c shows that ring 2 is in a very poor position to be attacked by C2, but in a good position to facilitate breaking either C3–C11 or C3–C31. Rings 1 and 3 need much less rotation to bond to C2. Figures 4d and 4b show that ring 3 would assist C3–C11 cleavage, and that ring 1 would assist C3–C21 cleavage. These notions are expressed more quantitatively in Table V. The second column gives the torsional angle between C2–C3 and the normal to the plane defined by the ipso and ortho carbons of each ring. Since the normal is near the direction of the ipso p orbital, bonding between C2 and C_{ipso} in the initial geometry should be related to this angle. Overlap should be approximately proportional to the cosine of the angle, so if the orbital interaction may be regarded as a perturbation, the stabilization should go as the square of the cosine, which value is given in parentheses. Attack on ring 3 is clearly preferred. Not only is its initial bonding to C2 one-third stronger than that from ring 1, but even more importantly, rotation of ring 1 to approach a spirocyclopropane geometry requires eclipsing C16–C11–C3–C31, while analogous rotation of ring 3 decreases the C32–C31–C3–C21 eclipsing.

It is risky to speculate about stabilization beyond the spirocyclopropane geometry, because torsional angles could change appreciably, but Table V also records for each ring the initial torsional angle between its bond to C3 and the axes of the ipso π orbitals of the other phenyls, defined by the ortho–ipso–ortho normal, as in the previous paragraph. In parentheses is given the square of the cosine of this angle as a rough estimate of the help each of the other rings might provide for breaking the bond between C2 and the ring in question. By this criterion migration of ring 1 should be strongly favored, but as mentioned above, we expect such help to become appreciable only after the rate-determining transition state.

On balance we conclude that intramolecular factors favor rearrangement of ring 3. Thus if the rigid matrix of TPPP influences the rearrangement of T by inhibiting changes in the phenyl group conformations, ring 3 should migrate. As an example of a type E, physical-mode effect, this result would be in accord with normal topochemical principles. To evaluate the possible consequences of other types of lattice influence we must examine the crystal packing.

Crystal Packing. TPPP molecules are shaped roughly like barbells elongated in the (11$\bar{1}$) direction of the lattice. They pack in columns in that direction, contacting one another across centers of symmetry so that the triphenylmethyl propellers of their "bells" intermesh. Columns which are neighbors along the *a* axis are offset along (11$\bar{1}$), the direction of the long molecular axis, by 4.43 Å, so that ring 1 in the "bell" of one column contacts two oxygens in the "bar" of the other. Similarly, columns which are neighbors in the *b* direction are offset by 5.15 Å, so that ring 2 in the "bell" of one column contacts two oxygens in the "bar" of the other. The center of symmetry between a molecule's peroxy oxygens means that each "bar" is surrounded by a belt of four aryl groups of TPPP, rings 1 along ±*a* and rings 2 along ±*b*. This packing mode leaves space between the chains which accommodates benzene of solvation. Six benzenes are near each "bar", but not so near as the four TPPP aryl groups. Packing around one "bar" is illustrated in Figure 5, and neighbor distances involving O1 and O2 are presented as Supplementary Material in Table XVII.

It is obvious that molecular species would not normally crystallize in a packing which shows the strong nonbonded repulsions required for important type A influence. However, a preliminary reaction, such as the photolytic double decarboxylation of TPPP, might easily be exothermic enough to generate enormous local repulsions, which could lead to type A influence on subsequent reaction steps. Figure 5 shows that there is no niche into which CO_2 may escape when TPPP undergoes double decarboxylation to generate the TT* radical pair. This means that until some cooperative motion in the lattice relaxes the strain from the new CO_2 molecules, their mutual repulsion will force them toward the T radicals, creating the possibility of a strong chemical-mode influence on the rearrangement.

Figures 5 and 4a suggest that CO_2 will be wedged between the CH_2 group and rings 2 and 3 of the T radical. This would obviously inhibit approach of C2 to the ipso carbon of ring 3. Furthermore, O1 is only 3.30 Å from C32 before decomposition. To the extent that O1 of the new CO_2 molecule is pressed even harder against that side of ring 3, it should prevent rotation of ring 3 in the direction necessary to increase its overlap with the radical orbital of C2. In both of these ways the CO_2 would inhibit ring 3 rearrangement by a type B influence. The inhibition is type B (chemical) rather than type D (physical), because the starting material is so close to the transition state that there is no room for an independent, physical transition state between them. Even very small motion of C2 toward the ipso carbon of ring 3 begins to change the bonding. Thus the influence of the CO_2 is on the

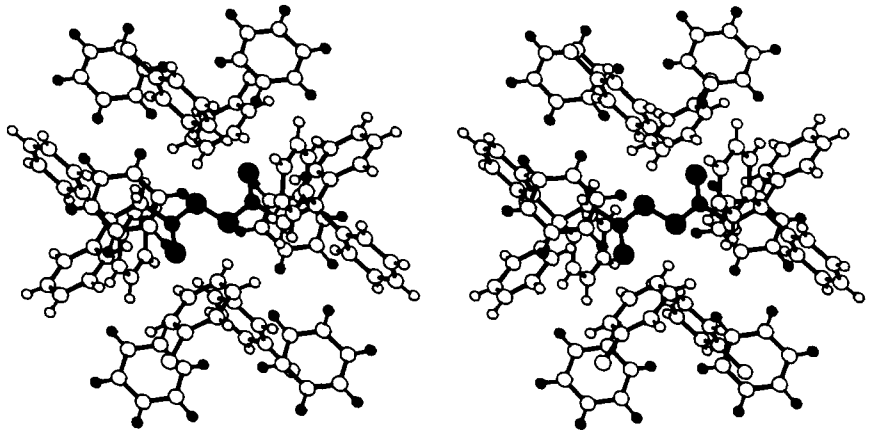

Figure 5. Environment of the peroxide bridge of TPPP. Atoms of the "S" shaped O=C—O—O—C=O bridge are darkened, as are the hydrogen atoms of benzene. The complete TPPP molecule is centered on (0,0,0). The coordinates of Table I are for atoms on the left half of this molecule and for the benzene molecule which partially obscures them. The nearest neighbors to the bridge are benzyl fragments of adjacent TPPP molecules. They can be identified because they are related by translation to corresponding fragments of the central TPPP. The benzyl fragment near the observer and low on the page is ring 2′ of the molecule related to the central molecule by translation along $+b$, while the fragment far from the observer and high on the page is ring 2 translated along $-b$. The fragment near the observer and high on the page is ring 1′ translated along a, while the fragment far from the observer and low on the page is ring 1 translated along $-a$.

normal, chemical transition state, not on preliminary motion necessary to achieve a geometry in which bonding change can begin.

No comparable intermolecular factor would militate against rearrangement of ring 1 in the strained geometry in which the radical pair should be created. In fact the new CO_2 should press C2 toward the ipso carbon of ring 1, thus favoring rearrangement. This assistance is a type A effect in which unusual strain in the starting material is relieved on approaching the transition state. Furthermore, Figure 5 shows that the benzene molecule touching the face of ring 1 does not block attack. It is far from C2 (H42–C2 is 4.15 Å, H43–C2 is 4.22 Å), and in fact H42 presses the edge of ring 1 in a way which should favor the rotation necessary to achieve better overlap between ring 1 and the radical center.

Thus we conclude that chemical-mode lattice influence of type A or type B, at least in the initial, strained geometry of the radical pair, should favor rearrangement involving ring 1. In the previous section we concluded that physical-mode influence of type D should favor rearrangement of ring 3.

Structure of the Radical Pairs. In the preceding paper we used hfs multiplicity, the rough magnitude of zfs, chemical conversions, and analogy to assign observed spectra to particular radical pairs in photolyzed crystals of TPPP. For each chemically distinct species, TT, TR, and RR, there were two different sets of signals, which we labeled TT and TT*, TR_1 and TR_3, and R_3R_1 and R_3R_3. The zfs and hfs tensors of Tables III and IV contain detailed structural information, which we may use to confirm the previous assignments and, more importantly, to discern differences between the structures of chemically equivalent radical pairs.

TT*. The first spectrum observed during low-temperature photolysis of TPPP comes from TT* and is characterized by its hfs tensor for splitting by four equivalent hydrogens and by its zfs tensor. Below 35 K the hydrogens seem to become inequivalent, but we have not determined their individual hfs. For the hfs tensors of the hydrogens in a single $-\dot{C}H_2$ group to be equivalent, the group must undergo rapid 180° rotation about the C–C bond. For the hfs tensor of one $-\dot{C}H_2$ within the TT* pair to be equivalent to that of the other $-\dot{C}H_2$, their axes of rotation must be nearly parallel or antiparallel. This is not surprising, since the environment of TPPP, the precursor molecule, is centrosymmetric.

Adrian, Bowers, and Cochran have discussed the hfs of $-\dot{C}H_2$ undergoing rapid 180° rotational jumps in the *n*-butyl and *n*-propyl radicals in an argon matrix at 4.2 K.[12] On average the isotropic hfs is −22.6 G, and the anisotropic eigenvalues are −6.2 G along the C–C axis, 1.6 G in the averaged direction of the radical p orbital, and 4.7 G in the third orthogonal direction. When our radical pair hfs data of Table IV are doubled for comparison with these tensors for isolated radicals, the agreement is reasonable. Our more positive value for a_{iso} may be due in part to the higher temperature of our experiment, and it is consistent with $a_{iso} = -10.9$ G for pairs of 2-phenylisobutyl radicals at 130 K[13] and with $a_{iso} = -21.85$ G for the same radical in solution at 237 K.[14] The 1.0 G difference between the positive eigenvalues for TT* is less than the expected half of the 3.1 G difference for the *n*-alkyl radicals, suggesting greater librational amplitude about the C–C bond in TT*. A root mean square value of 0.82 for the cosine of the librational amplitude in T would explain so small a difference, but we assign little significance to this number, which is the cosine of 32°.

On the other hand, it seems unlikely that libration should be freer in TT* if 180° rotation is frozen at 34 K[15] while it persists to 4.2 K for the simple alkyl radicals in argon. An alternative explanation for the smaller departure from cylindrical symmetry in the hfs tensors is that centrosymmetry is broken to given somewhat different average $-\dot{C}H_2$ torsions in the two T radicals. The overall hfs from a pair of such methylene groups would be closer to cylindrical symmetry, but we did not detect line width variation within the hfs quintuplet, which a substantial difference in average torsional angle would have required.

The direction of the hfs eigenvectors is more significant than their precise magnitude, because the most negative eigenvector shows the direction of the C3–C2 bond in the free radical, and the intermediate eigenvector shows the direction of its nonbonding p orbital. If we assume temporarily that the triphenylmethyl portion of T remains anchored at the position it occupied in TPPP, and that the C3–C2 distance in T is 1.47 Å, then these two directions allow us to locate the $-\dot{C}H_2$ group and to determine its conformation. The first row of Table VI gives the calculated location of C2 both in Cartesian coordinates and in cylindrical polar coordinates for use with Figure 4a. The calculated position of C2 in the radical pair is only 0.11 Å from its position in TPPP, and most of this displacement is due to assumed shortening of C2–C3. For comparison, the radius of circles denoting carbon in Figure 4 is 0.30 Å. The change in direction of C3–C2 from TPPP to T is only 2.6°.

The direction of the p orbital is such that one of the CH_2 hydrogens eclipses C3–C21. This could give favorable homo-

(12) (a) Adrian, F. J.; Cochran, E. L.; Bowers, V. A. *J. Chem. Phys.* **1973**, *59*, 3946. (b) Adrian, F. J.; Bowers, V. A.; Cochran, E. L. *Ibid.* **1975**, *63*, 919.

(13) In a photolyzed single crystal of 3-methyl-3-phenylbutanoyl peroxide. McBride, J. M., unpublished work in this laboratory.

(14) Hamilton, E. J., Jr.; Fischer, H. *Helv. Chim. Acta* **1973**, *56*, 795.

(15) Note that the apparent change in hfs at low temperature may be due to incomplete averaging of zfs rather than of hfs.

Table VI. Inferred Positions for C2 of T Radicals[a]

pair	source[b]	a	b'	c^*	r	l	θ, deg	d_{C_2}[c]	d_{C_3}[d]
TT*	hfs	2.45	1.07	−1.27	0.07	0.09	273	0.11	[1.47]
	zfs	2.63	1.22	−1.27	0.16	0.21	152	0.23	1.36
TT	hfs	2.53	1.03	−1.27	0.12	0.09	229	0.15	[1.47]
	zfs	2.61	1.15	−1.25	0.14	0.15	169	0.21	1.41
TR_3	hfs	2.22	1.37	−1.22	0.33	0.13	35	0.36	[1.47]

[a] The coordinates of C2 are given in two systems: (1) a, b', c^*, the orthogonal crystal coordinates; and (2) r, l, θ, which are cylindrical polar coordinates for use with Figure 4a, where r is the distance from the C2–C3 axis, l is the distance of the point's projection on that axis from C2 (positive toward C3), and θ is the torsional angle C1–C2–C3–X (positive for clockwise rotation from C1 in Figure 4a). All distances are in angstroms. [b] Tensor used to determine position. For TT* the hfs and zfs results differ by 0.23 Å, and for TT by 0.15 Å. The amount of C2 motion from TT* to TT is 0.09 Å by hfs or 0.07 Å by zfs. By hfs the C2 position in TR_3 is 0.37 Å from that in TT* and 0.46 Å from that in TT. [c] Distance from C2 of the precursor TPPP molecule (Å). [d] Distance from C3 of the precursor (Å). The values in brackets were assumed.

conjugation with ring 2, but through-space overlap with ring 3 might also be important, and it is difficult to know what role the CO_2 molecule might play in determining the $-\dot{C}H_2$ conformation.

While hfs determines the location of C2 relative to C3, zfs determines its position relative to C2 of the other radical in the pair. This relative position takes on absolute significance if we assume preservation of centrosymmetry. In interpreting the zfs, we assume further that the spin density of C2 can be approximated by two half-spins flanking C2 at ±0.65 Å in the direction of the p-orbital axis, which was determined above from hfs. The position of C2 was adjusted to minimize the root mean square difference between observed and calculated elements of the zfs tensor. For the position given in the second row of Table VI the root mean square difference is 1.8 G, and it grows to more than 2.5 G for displacement by 0.05 Å in any direction. The position is moderately sensitive to the assumed extension of the p orbital, varying by ±0.15 Å for half-spin displacements in the range 0.85–0.45 Å.

The C2 positions determined by hfs and by zfs differ by 0.23 Å, which is slightly beyond reasonable error limits. The most likely explanation for this discrepancy is that C3 in the radical is displaced by 0.1 to 0.2 Å from its position in TPPP in a direction away from CO_2. The small size of the C2 and C3 displacements confirms the identity of TT* and shows that the T radicals are firmly anchored in the crystal lattice.

TT. Above 150 K TT* converts irreversibly to TT with an activation energy of 9.6 kcal/mol.[4] Table X gives the C2 positions derived from the zfs and hfs tensors as for TT*. The zfs tensor was simulated with a root mean square deviation of 0.7 G. Again the C2 position is within 0.25 Å of that for the precursor molecule, TPPP. Although the necessity for assumptions casts some suspicion on the precision of these positions, experiment leaves no doubt on four points: (1) the C2 atoms of TT are 0.09 ± 0.01 Å *closer together* than those of TT*, (2) the C2–C2 interradical direction changes by less than 2° between TT and TT*, (3) the C2–C3 bond directions change by only 4 ± 2°, and (4) torsion of the $-\dot{C}H_2$ group changes by only 8 ± 6°.

The motions of C2 and C3 on conversion of TT* to TT are less than their root mean square amplitude of thermal vibration in TPPP. For TT* and TT to represent independent species separated by a 9.6 kcal/mol barrier, the difference in their structures must be much greater than appears from the positions of C2 and C3. There must be a substantial change in the structure of the rest of the radical, or more probably in that of the environment.

Driving force for the structural change must come from release of the strain created by converting bonded CO_2 groups of TPPP into free CO_2 molecules wedged between the radicals of TT*. Although the motion we see is too subtle to interpret confidently, the decreased C2–C2 separation of TT suggests that the CO_2 molecules shift aside from their initial position in which they pressed the radicals apart. By examining Figure 5 the reader can guess as well as we can whether CO_2 motion is permitted by a change in conformation of a neighboring TPPP molecule or by motion of one of the neighboring benzenes of solvation. It could well be that most of the motion necessary for relaxation occurs in one member of the radical pair. In this case centrosymmetry would be lost, and the moving radical would have to move twice as far to achieve the relative motion we observe. A molecular mechanics calculation might shed some light on this question.

TR_1. For two reasons it is much more difficult to interpret the structural information in the tensors of TR pairs than in those of TT pairs. First, it is obviously impossible to determine absolute positions from the zfs by assuming centrosymmetry, as we did for TT. This does not hinder qualitative interpretation, however, because we can assume that if C2 of a T radical moves less than 0.25 Å on formation of TT* from TPPP and during lattice relaxation from TT* to TT, it also moves very little on subsequent rearrangement of the radical with which it is paired. This provides a fixed point for the spin of T from which zfs will measure the approximate absolute position of the spin on R.

The second difficulty is more troublesome. Magnetic interactions depend on spin distribution, and spin on the doubly benzylic radical R should be delocalized over many atoms. Not only do the five independent elements of the zfs tensor lack sufficient information to determine the position of many atoms, but the atomic spin densities in R are hard to guess. Spin densities at the α carbons of benzyl and diphenylmethyl have been measured as 0.61 and 0.54, respectively,[16] but the phenyl conformations may be unusual in our trapped radicals. Both conformations and spin densities should be accessible through ENDOR, but we have not made such measurements. Instead we have constructed plausible models for the structure and spin distribution of the three different R radicals which would result from rearrangement of the three different phenyl rings. We named the models R1, R2, and R3, according to the number of the rearranged phenyl ring, and we used them to evaluate the observed zfs and hfs tensors qualitatively. Note the difference between the names of the models and those of the experimentally observed species, which bear numerical subscripts.

The models assume that the R radicals have normal bond lengths and angles and that the centers of the phenyl rings remain stationary during rearrangement, so that R can fit into the cavity which accommodated TPPP and T. Thus C3 is 2.85 Å (phenyl radius + 1.45 Å) from the center of each benzylic ring, while C2 is 2.94 Å (phenyl radius + 1.54 Å) from the center of the rearranged ring, 1.47 Å from C3, and equidistant from the centers of the benzylic rings. The bond angles at C2 are kept tetrahedral.

These constraints fix C2 and C3 at the positions given in Table VII. They do not permit planarity at C3, but the amount of distortion shown in Table VII may be realistic, since out-of-plane distortion of the *tert*-butyl, a nonconjugated radical, is so facile.[17] Because the centers of rings 1 and 2 in TPPP are closer to each other (4.57 Å) than either is to that of ring 3 (4.98, 4.97 Å,

(16) Park, J. M.; McDowell, C. A. *Mol. Phys.* **1976**, *32*, 1511. Cf.: Jones, P. R.; Wood, D. E.; et al. *J. Am. Chem. Soc.* **1975**, *97*, 4477. (b) Bassingdale, A. R.; et al. *Tetrahedron Lett.* **1973**, 3185.

(17) Griller, D.; Ingold, K. U.; Krusic, P. J.; Fischer, H. *J. Am. Chem. Soc.* **1978**, *100*, 6750.

(18) Fischer, H. In "Free Radicals", Kochi, J. K., Ed.; Wiley: New York, 1973; Vol. II, Chapter 19. Gilbert, B. C.; Trenwith, M.; Dobbs, A. J. *J. Chem. Soc., Perkin Trans. 2* **1974**, 1772. Division by 2 corrects from isolated radicals to radical pairs.

Table VII. Geometry and Spin Distribution of the R Models[a]

		R1	R2	R3
position of C3	*a*	2.17	2.92	3.20
	b'	2.01	1.08	1.97
	*c**	−2.24	−2.44	−1.81
position of C2	*a*	3.13	2.46	2.06
	b'	1.16	1.98	1.05
	*c**	−1.53	−1.37	−1.81
distance of C3 from the plane of the adjacent atoms, Å		0.28	0.29	0.26
bond angles at C3, deg		121	122	107
		114	113	122
		114	113	123
spin densities[b]	C3	0.55	0.55 (0.55)	0.75 (0.59)
	ring 1		0.35 (0.10)	0.10 (0.18)
	ring 2	0.10		0.15 (0.23)
	ring 3	0.35	0.10 (0.35)	

[a] Each column gives parameters for one model. [b] Alternative spin density assignments are given in parentheses.

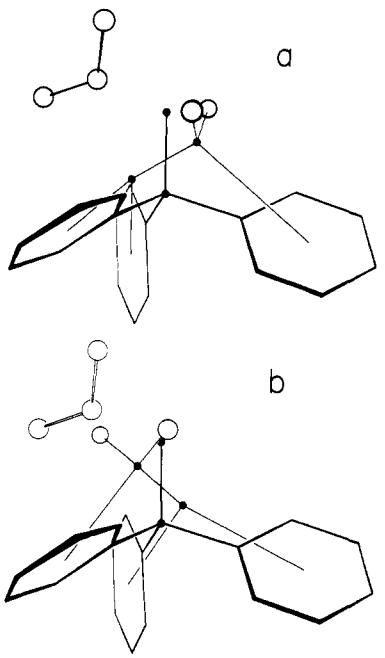

Figure 6. Models R1 and R3 (a and b, respectively) superimposed on the T CO_2 framework of their TPPP precursor. C2 and C3 are indicated by filled circles, while the hydrogens of C2 and the atoms of CO_2 are indicated by open circles. The CO_2 in b is drawn lightly, because we believe it must move before R3 may form. Ring 1 projects to the right; ring 2, into the page; and ring 3, toward the reader. Note that the motion involved in rearrangement from T to R is primarily rotation of the C2–C3 fragment, and that in R the bonds from C3 are not coplanar.

respectively), the models for rearrangement of rings 1 and 2 have C2–C3 torsional angles which are 8° from the symmetrical staggered conformation. The locations of C2 and C3 in models R1 and R3 are illustrated in Figure 6. In each of the models C3 is 0.75 ± 0.01 Å from its position in TPPP and 1.16 ± 0.05 Å from C3 of the other two models for rearranged radicals. For C2 the corresponding figures are 0.83 ± 0.09 and 1.09 ± 0.02 Å. Since C3 bears most of the spin and C2 bears the β hydrogens, these differences have obvious implications for the orientation of the zfs and hfs. Contrary to our intuition, the amount of atomic motion required for rearrangement is in fact quite small. It consists primarily of a rotation of the C2–C3 fragment by some 50° with minor adjustment of the phenyl orientations.

Table VIII. Comparison of Model and Experimental zfs Tensors for the TR Pairs

	model[b]			exptl	
parameter[a]	TR1	TR2	TR3	TR_1	TR_3
magnitude of D_{neg}	154	122 (140)	125 (113)	137	88
angle of D_{neg} from TR_1	3	14 (10)	17 (16)		11
angle of D_{neg} from TR_3	9	7 (10)	6 (6)	11	
$D_{pos} - D_{int}$	9.5	3.8 (8.8)	1.9 (3.0)	9.5	1.7
angle of D_{pos} from TR_1	12	23 (18)	84 (84)		54
angle of D_{pos} from TR_3	42	74 (72)	31 (30)	54	

[a] D_{neg} and D_{pos} are the maximum negative and positive splittings of the zfs doublet in gauss. D_{int} is the splitting with the magnetic field in the third orthogonal direction. Eigenvalues of the D tensor are one-third as large as thses splittings. The angular divergences in degrees are between the eigenvector calculated from the model and that observed experimentally for the indicated pair. [b] Results for the TR2 and TR3 models with the alternative spin distributions of Table VII are given in parentheses.

Table IX. Comparison of Model and Experimental hfs Tensors for the TR Pairs

		angle from[a]			
model	proton	$TR_1\beta_1$	$TR_3\beta_1$	$TR_3\beta_2$	a_{1SO}[b]
R1	1	2	78	86	5.4
R1	2	29	61	67	2.6
R2	1	28	54	52	5.4 (5.4)
R2	2	2	75	80	2.6 (2.6)
R3	1	65	32	34	5.4 (4.2)
R3	2	64	26	19	5.2 (4.1)

[a] Angular divergence (deg) between the most positive eigenvector of the experimental hfs tensor and the vector from the indicated proton to C3 of the model. This type of comparison is crude but adequate given our experimental precision. [b] a_{1SO} (gauss) was calculated for the model by the formula given in the text. The experimental values for $TR_1\beta_1$, $TR_3\beta_1$, and $TR_3\beta_2$ are 6.9, 5.5, and 1.1 G, respectively.

In each model we distributed unit spin density among C3 and the centers of the two conjugated rings. The distribution was guessed on the basis of three considerations: (1) the atomic spin densities in benzyl[16a] and in diphenylmethyl;[16b] (2) the potential for delocalization of each phenyl after rearrangement, as suggested by the conformations in Figure 4; and (3) the amount of departure from cylindrical symmetry in each of the observed zfs tensors. The assumed spin distributions are shown in Table VII. The modest change in calculated tensors for the substantial changes to the alternative spin distribution for R2 and for R3 (see Table VIII) suggests that the models should suffice for qualitative interpretation.

Comparison of calculated with experimental zfs eigenvectors (Table VIII) convinces us that ring 1 migrates during photolytic formation of TR_1 from TT*. This is why the experimental pair was named TR_1. The calculated maximum zfs for TR1 is larger than the experimental, but increasing the radical–radical separation from 6.71 to 6.98 Å would correct the calculated value. The field direction for maximum zfs is decisive. The experimental direction diverges by only 3° from TR1 (which corresponds to a shift of 0.36 Å in the relative positions of the radicals), but by more than 10° for the other models. Furthermore the TR1 model predicts both the magnitude and the direction for the tensor's substantial departure from axial symmetry, which results primarily from spin delocalization into ring 3.

The TR3 model is obviously inconsistent with the experimental zfs of TR_1. The TR2 model is not so bad as TR3, but it is markedly inferior to TR1. Even if we shift as much spin density to ring 3 of TR2 as we assigned to that ring in TR1, the zfs angular errors remain large. For example, the 10° error in the direction of maximum zfs could be corrected only by 1.19 Å relative motion of the radicals. The conformation of ring 2 in TPPP also makes the TR2 model mechanistically implausible, as discussed above.

The hfs evidence in Table IX is consistent with our identification of TR_1. The torsion about C2–C3 in R1 predicts one large and

Table X. Comparison of Model and Experimental zfs Tensors for the RR Pairs

		D_{neg}			D_{pos}, D_{int}		
			angle from[c]			angle from[e]	
model	C3–C3 dist,[a]	size[b]	R_3R_1	R_3R_3	diff[d]	R_3R_1	R_3R_3
R1R1	7.4	95	2	18	8	31	48
R1R2	7.6	83	7	12	4	17	61
R1R3	7.8	89	6	6	3	36	43
R2R2	7.9	68	16	14	3	12	82
R2R3	8.0	73	14	5	1	23	81
R3R3	8.3	74	18	6	2	78	25

[a] Distance (Å) between the benzylic carbons of the model. [b] Maximum (negative) value of the splitting of the spectral doublet in gauss. The negative eigenvalue of the D tensor is one-third of this value. The observed values are 65 G for R_3R_1 and 45 G for R_3R_3. [c] Divergence in degrees between the negative eigenvectors calculated from the models and those observed experimentally. The divergence between the experimental eigenvectors in 12°. [d] Range (in gauss) of spectral splittings observed with the applied field perpendicular to the direction of maximum splitting. The observed ranges are 8 G for R_3R_1 and 2 G for R_3R_3. [e] Average divergence in degrees between calculated and observed directions of the two positive eigenvectors. The average divergence for the two experimental tensors is 78°.

one small isotropic hfs for the β hydrogens. The calculated magnitudes are roughly correct, although the formula by which they were estimated, a_{iso} (Gauss) = $(3.2 + 43.5\cos^2\theta)\rho/2$, applies properly only to radicals with planar centers.[18] The first column of angles in Table IX shows that only proton 1 of model R1 and proton 2 of model R2 are close to the observed direction from the adjacent radical center. The R2 possibility is excluded by the small predicted a_{iso}.

TR_3. The zfs data of Table VIII are consistent with both TR2 and TR3 as models for TR_3. The TR3 model fits the small departure from axial symmetry better than TR2 does, but the difference is unconvincing because of experimental uncertainty. In either model the radicals must separate by another 0.5 to 0.7 Å to explain the small maximum zfs observed experimentally.

A clear choice in favor of TR3 is possible on the basis of hfs anisotropy, which is experimentally more reliable for TR_3 than for TR_1. For the β hydrogens the direction of maximum splitting is in error by 19° and 32° for the TR3 model, but by 52° and 75° for TR2. The difference in a_{iso} for the B hydrogens shows that the true R_3 radical is twisted about C3–C2 by perhaps 10° from the staggered geometry of the R3 model.

The hfs tensor for the α hydrogens of T in the TR_3 pair is similar to those in TT* and TT, but less reliably determined. The unique eigenvector suggests that the direction of C3–C2 changes from TPPP by 13°, as shown by the last row of Table VI. This probably indicates a modest reorientation of the T radical as a whole.

RR. The strongest argument for assigning chemical structures to the RR signals comes from analogy, they grow at the expense of TR under the same conditions, thermal or photolytic, which cause TR to grow at the expense of TT. hfs provides only the support of negative evidence, namely that there is no resolved splitting from α hydrogens. In fact there is only a broad envelope from multiple unresolved hfs, which narrows on deuteration.

The zfs tensors contain some structural evidence. Table X compares experimental zfs parameters with those calculated for all pairs of our models for rearranged radicals. There are four comparisons: the magnitude of the largest (negative) splitting, and its direction; and the difference between the positive splitting eigenvalues, and their directions. In each case the directions are reported relative to the corresponding eigenvectors of the experimental RR tensors. The negative eigenvector is primarily dependent on the separation of the radicals, while the difference of the positive eigenvectors is primarily dependent on delocalization within the radicals.

The negative zfs maxima clearly distinguish the two experimental RR pairs, but they do not permit a choice among the models, because both of the observed values are smaller than any of the models predict. This suggests that the true radicals are 10 to 20% (0.8 to 1.4 Å) further apart than the models show. It is suggestive that all of the models which include an R1 radical have large zfs maxima compared to all the models which do not, and that one of the experimental tensors has a much larger zfs maximum than the other.

Stronger evidence that the species we label R_3R_1 include an R1 radical comes from the orientation of the maximum zfs eigenvector. The models including an R1 radical give vectors within 7° of the observed vector, while models lacking an R1 give vectors deviating by 14° to 18° (1.9 to 2.6 Å).

The same line of evidence indicates that the R_3R_3 species contains an R3 radical. Models including R3 give vectors deviating from that of R_3R_3 by 6° or less, while those lacking an R3 deviate by 12° to 18° (1.6 to 2.3 Å).

Of course it comes as no surprise that R_3R_1 should contain an R1, since its precursor is TR_1. It is similarly reasonable that rearrangement of TR_3 should give an RR pair including R3. Unfortunately the models are not sufficiently realistic to be confident about the subscript of the other rearranged radical in each of the RR pairs. We have guessed that the other radical is R3 because this is the radical we would expect from rearrangement in an unstrained environment, as discussed above. Data in the last three columns of Table X favor R3R3 for R_3R_3 and R1R1 for R_3R_1, but the experimental values are too uncertain for this evidence to be given much weight.

Conclusions

The above results show conclusively that degeneracy of the neophyl rearrangement of T is lifted in crystalline TPPP, and that the structure of the precursor radical pair and its environment, not the thermal or photochemical method of stimulating rearrangement, determines which phenyl will migrate. Given the large number of possible radical pairs from this complex system, it is remarkable that all of the pair signals we have observed below 200 K can be assigned to one of the six pairs discussed above.

When rearrangement occurs in the relaxed geometry of pair TT, it yields the topochemical product, TR_3. As far as selectivity among the phenyl groups is concerned the matrix plays only the indirect, secondary role of preventing their conformational equilibration. The selectivity is as expected for a radical of this conformation in the gas phase. A type E, physical mode of influence is sufficient to explain the selectivity. Of course the significant retardation of rearrangement which we observe demands in addition a direct, chemical mode of influence of type B. Type D retardation is not possible because of the proximity of starting material to transition state in this rearrangement.

The situation is completely different for rearrangement of the strained TT* pair. Although the conformation of the T radicals in this pair is presumably such as to favor rearrangement of ring 3 (both TPPP, the precursor of this pair, and TT, its thermal successor, have this conformation), ring 1 in fact rearranges. In order to make the reaction take this unnatural course the lattice must be playing an active, direct role in its chemistry.

We discussed above how pressure of a CO_2 molecule against C2 should accelerate rearrangement of ring 1 by a mechanism of type A and retard that of ring 3 by one of type B. Unfortunately we cannot distinguish these mechanisms by measuring the rate of thermal rearrangement of TT*, because relaxation to TT is faster than thermal rearrangement, so that only low-temperature photochemical rearrangement can be observed. The similarity of rate between relaxation of TT* and rearrangement of TT (which is slow compared to solution rearrangement) suggests that type A acceleration is not overwhelmingly large.

Whether rearrangements of TT* is subject to type A or type B influence or, as seems most likely, to both, it constitutes a clear example of the chemical mode of lattice control over a solid-state reaction. From a simplistic point of view it is a violation of the topochemical rules, in that the rearrangement takes a course contrary to that which the radical's solid-state conformation should favor.

The amount of structural and kinetic detail which EPR has supplied for this system involving six different radical-pair intermediates shows why this approach is particularly appealing for studying the nature of reactions in organic solids. One might think that the substantial lattice strain which is generated during radical-pair formation would make this type of reaction a poor model for solid-state reactions in general, but it could equally well be that hypothetical reaction in an unstrained lattice is in fact the poor model. Only the first molecule to react in a perfect crystal could react in a truly strain-free environment. All molecules reacting subsequently should be more or less sensitive to strain generated by earlier events, and the type of strain effects revealed in the present work may be widespread in solid-state chemistry.

There are a number of directions in which this work could be profitably extended. Molecular mechanics could yield insight on the nature of intermolecular interactions in these crowded cages. ENDOR spectroscopy could give more geometric detail on the structure of the rearranged radical pairs. Analysis of the ultimate products is obviously necessary, especially since some of the pair-pair conversions are not quantitative. We have made preliminary attempts to study other solvates of TPPP, but the crystals we could grow from chloroform, chlorobenzene, acetone, ethyl acetate, and ether were either microcrystalline or needles too fine for single-crystal EPR investigation.

Experimental Section

Preparation of the compounds and operation of the EPR spectrometer was described in the preceding paper.[4] The method for determining hfs and zfs tensors has been previously described.[19]

X-ray Data were collected on a crystal 0.3 mm on each edge mounted in a sealed quartz capillary. The Enraf-Nonius CAD-4 diffractometer used Mo Kα irradiation with a graphite monochromator and pulse height discrimination. Lattice parameters were refined on the basis of 25 reflections with $6° < \theta < 19°$. Intensity data were collected using ω-2θ scans over an ω range of $(0.75 + 0.35°) \tan(\theta)$, slow enough to give $\sigma(I)/I = 0.02$ but not exceeding 60 s. Three standard reflections were monitored after each 10^4 s of X-ray exposure and showed less than 8% variation during data collection. Structure factors were calculated for the 2434 unique reflections after Lorentz-polarization and background corrections. Reflections were weighted according to a standard scheme.[20] The 2243 reflections with $I > 2\sigma(I)$ were used in structural refinement.

The structure was solved by direct methods and refined using the 1977 version of the Enraf-Nonius SDP package. Positional parameters of all atoms, isotropic thermal parameters for the hydrogens, and anisotropic thermal parameters for all other atoms were varied in the final refinement cycles to minimize $\sum w(|F_o| - |F_c|)^2$. The final values of R and of $R_w = [\sum w(|F_o| - |F_c|)^2/\sum wF_o^2]^{1/2}$ were 0.051 and 0.057, respectively.

Acknowledgment. This work was supported by the National Science Foundation (DMR 76-01996) and in its early stages by a Camille and Henry Dreyfus Teacher-Scholar Grant. The EPR spectrometer and the X-ray diffractometer were obtained with the aid of NSF departmental instrument grants. J.M.M. is grateful for the hospitality of Professor J. M. Thomas, University of Cambridge, and for a Senior Visiting Fellowship from the Science Research Council of Great Britain during preparation of the manuscript.

Supplementary Material Available: Thermal parameters and rms vibrational amplitudes, observed and calculated structure factors, bond lengths, bond angles, least-squares planes, torsional angles, nonbonded distances from O1 and O2 (14 pages). Ordering information is given on any current masthead page.

(19) Karch, N. J.; Koh, E. T.; Whitsel, B. L.; McBride, J. M. *J. Am. Chem. Soc.* **1975**, *97*, 6729.

(20) Stout, G. H.; Jensen, L. H. "X-ray Structure Determination"; Macmillan: New York, 1968; p 457.

Mercaptide-Chelated Protoheme. A Synthetic Model Compound for Cytochrome P-450[1]

T. G. Traylor,* Terry C. Mincey, and Albin P. Berzinis

Contribution from the Department of Chemistry, University of California, San Diego, La Jolla, California 92093. *Received January 30, 1981*

Abstract: A synthetic protohemin compound having a covalently attached and protected mercaptide function has been prepared. Reduction of the hemin and deprotection of the mercaptide in alkaline aqueous suspension (cetyltrimethylammonium bromide) or in dimethyl sulfoxide solution afforded mercaptide-chelated protoheme which displays the spectroscopic properties of cytochrome P-450. Nuclear magnetic resonance spectra of the carbon monoxide complex of this model compound display new resonances in both proton NMR and ^{13}CO NMR which serve to confirm the structure and to afford new probes for studies of the proteins themselves. Kinetics and equilibria of CO binding of this model compound in aqueous suspension indicate that the model has lower affinity for CO than does cytochrome P-450, suggesting that the charge on the sulfur may be reduced in the protein.

Comparisons of UV-visible, Mössbauer, ESR, and other spectra of cytochromes P-450 with those of model systems have provided strong evidence for the presence of a mercaptide-iron bond in at least some forms of the P-450 enzyme.[2,3] Except for the crystal structure study of protohemin dimethyl ester *p*-nitrothiophenolate,[4] all these model systems have consisted of solutions of heme (or hemin) in the presence of rather large concentrations (0.001-0.1 M) of excess mercaptide ion.

Although static, spectroscopic properties of such model systems are not affected by this excess base (RS^-), dynamic properties could be greatly affected as they are with other bases such as

(1) A preliminary report of a similar mercaptide-chelated heme has appeared.[2]

(2) Traylor, T. G.; Mincey, T. *Acta Biol. Med. Ger.* **1979**, *38*, 351-355.

(3) Chang, C. K.; Dolphin, D. In "Bioorganic Chemistry"; van Tamelen, F. E., Ed.; Academic Press: New York, 1978; Vol. 4, pp 37-80. This review describes the cytochrome P-450 model studies.

(4) (a) Tang, S. C.; Koch, S.; Papaefthymiou, G. C.; Foner, S.; Frankel, R. B.; Ibers, J. A.; Holm, R. H. *J. Am. Chem. Soc.* **1976**, *98*, 2414-2434. (b) Debrunner, P. G.; Gunsalus, I. C.; Sligar, S. G.; Wagner, G. C. In "Metal Ions in Biological Systems"; Sigel, Ed.; Marcel Dekker: New York, 1978; Vol. 7, pp 241-275.

0002-7863/81/1503-7084$01.25/0